Spatial structure of spin polarons in the *t-J* model

A. Ramšak

Max-Planck-Institut für Festkörperforschung, D-70569 Stuttgart, Federal Republic of Germany;
Faculty of Mathematics and Physics, University of Ljubljana, SI-1000 Ljubljana, Slovenia;
and J. Stefan Institute, SI-1000 Ljubljana, Slovenia

P. Horsch

Max-Planck-Institut für Festkörperforschung, D-70569 Stuttgart, Federal Republic of Germany
(Received 23 September 1997)

The deformation of the quantum Néel state induced by a spin polaron is analyzed in a slave fermion approach. Our method is based on the self-consistent Born approximation for the Green's function and wave function for the quasiparticle. The results of various spin-correlation functions relative to the position of the moving hole are discussed and shown to agree with those available from small cluster calculations. Antiferromagnetic correlations in the direct neighborhood of the hole are reduced, but they remain antiferromagnetic even for J as small as $0.1t$. These correlation functions exhibit dipolar distortions in the spin structure, which sensitively depend on the momentum of the quasiparticle. Their asymptotic decay with the distance from the hole is governed by power laws, yet the spectral weight of the quasiparticles does not vanish. [S0163-1829(98)03008-2]

I. INTRODUCTION

The problem of spin polarons moving in a quantum anti-ferromagnet has received considerable attention, since it is important for a description of Mott insulators at low doping.[1] While the major part of investigations for the *t-J* model was concerned, e.g., with the polaron dispersion and spectral function using a variety of techniques such as exact diagonalization,[2–7] self-consistent Born approximation (SCBA),[8–11] string theory,[12,13] and other methods[14–17]—our focus here is on the spatial structure of the spin polarization and its asymptotic behavior. The study of the deformation of the spin system due to spin-polaron formation was mainly performed by exact diagonalization techniques.[3,18] However, there are important questions which can only be studied by analytical approaches, such as the asymptotic decay of the polarization of the medium.[19,20] The latter property is closely related to the question whether a quasiparticle (QP) description applies. The first successful measurement of single-hole dispersion in the Mott insulator $Sr_2CuO_2Cl_2$ by angular-resolved photoemission[21] revived this interest, and stimulated investigations of the *t-t'-J* model[22] and more complex Hamiltonians.[23]

The Green's function for a hole moving in a *fixed* spin background was already discussed in the context of transition-metal oxides by Bulaevskii, Nagaev, and Khomskii[24] in the late 1960s, and by Brinkman and Rice.[25] In those approaches the Green's function turned out to be local and fully incoherent. The first prediction that low-energy single-particle excitations in the two-dimensional (2D) *t-J* model[26] and its anisotropic generalization ($0 \leq \alpha \leq 1$),

$$H_{t\text{-}J} = -t \sum_{\langle ij \rangle \sigma} (\widetilde{c}_{i,\sigma}^\dagger \widetilde{c}_{j,\sigma} + \text{H.c.})$$
$$+ J \sum_{\langle ij \rangle} \left[S_i^z S_j^z + \frac{\alpha}{2}(S_i^+ S_j^- + S_i^- S_j^+) \right], \quad (1)$$

are propagating QP's with a bandwidth of order J was made by Kane, Lee, and Read,[9] and was confirmed by a number of exact diagonalization studies.[2,3] The problem is complicated due to the constraint on the fermion operators $\widetilde{c}_{i,\sigma}^\dagger = c_{i,\sigma}^\dagger (1 - n_{i,-\sigma})$, and by the fact that quantum fluctuations play a crucial role. This model was widely studied particularly because it is believed to contain much of the low-energy physics of the high-T_c superconductors.[26,1]

Nevertheless, fundamental issues are still unclear, such as the spin dynamics and the form of the Fermi surface at moderate doping, i.e., in the regime corresponding to underdoped high-temperature superconductors. However, even in the case of a single hole there are different views, e.g., whether the quasiparticle spectral weight is finite or vanishes in the thermodynamic limit. In particular, Anderson argued that holes introduce a deformation in the spin background which decays as a power law and as a consequence the spectral weight should vanish, leading to non-Fermi-liquid behavior.[27] According to this argument, non-Fermi-liquid behavior is connected with the property of a single hole. Recently, Weng *et al.*[28] argued that the quasiparticle weight $Z_{\mathbf{k}}$ should vanish as a consequence of string formation associated with the Marshall's sign, which is a characteristic property of the undoped Heisenberg ground state. These arguments are based on the appearance of an orthogonality catastrophe in the matrix element $\langle \Psi_{\mathbf{k}}^{\text{exact}} | c_{\mathbf{k}\sigma} | 0 \rangle$, between

the exact, i.e. fully relaxed, single-hole ground state, and the state $c_{\mathbf{k}\sigma}|0\rangle$, where $|0\rangle$ is the ground state of the Heisenberg model without holes.

The asymptotic decay of the polarization cloud cannot be analyzed by numerical methods, such as exact diagonalization (quantum Monte Carlo results for the 2D t-J model are still not available), since such studies are confined to small clusters and thus can only provide insight into the short-range deformation of the spin background.

A particularly powerful tool in the study of the spin polaron problem is the slave fermion approach combined with a self-consistent Born approximation for the calculation of the polaron Green's function.[8,9] This approach was successful in reproducing the diagonalization results for the full Green's function obtained by diagonalization.[2] Therefore we shall follow this route here. Furthermore the method properly accounts for the low-energy spin excitations, which are crucial for the long-range distortion of the spin-background around the moving hole. This method has also been applied to the finite doping case.[29–31] A further important step was the explicit construction of the quasiparticle wave function within the SCBA by Reiter.[32] This wave function implicitly contains all information about the deformation of the spin system, and can be used to calculate this perturbation in terms of correlation functions.

Of particular interest is here the study of relative correlation functions (RCF's), i.e., relative to the position of the hole, as for example $C_{\mathbf{R}}=\langle n_0(\mathbf{S}_{\mathbf{R}_1}\cdot\mathbf{S}_{\mathbf{R}_2})\rangle$, which measures the nearest-neighbor correlation function for a bond at a distance $\mathbf{R}=(\mathbf{R}_1+\mathbf{R}_2)/2$ from the hole at $\mathbf{R}=0$ (assuming here that $\mathbf{R}_1$ and $\mathbf{R}_2$ differ by a lattice unit vector $\mathbf{u}$). Such correlation functions are usually not studied because of their complexity. However, they provide detailed information about deformation of the spin system around the moving hole, in contrast to the averaged correlation function $\langle\mathbf{S}_{\mathbf{R}_1}\cdot\mathbf{S}_{\mathbf{R}_2}\rangle$, which measures only the global change in spin correlations due to the holes.

The results for the RCF's clearly show that nearest-neighbor spin correlations in the neighborhood of the hole are reduced, yet they remain antiferromagnetic (even for J as small as $0.1t$). Therefore the frequently invoked ferromagnetic polaron picture, where the hole is assumed to move in a ferromagnetically aligned neighborhood of spins, does not apply to the t-J model.

The main purpose of this work is to use Reiter's wave function for the calculation of correlation functions, and to present a quantitative picture of the shape and size of the quasiparticle. While a short summary of selected results was given earlier,[20] the present work focuses on the description of the technique employed for the calculation of the correlation functions. The technique discussed here may also be useful in other cases where the noncrossing approximation is employed, such as more complex models including electron-phonon coupling.[33,34] Results for various correlation functions describing the deformation of the spin background around the hole will be presented for the t-J model [$\alpha=1$ in Eq. (1)], as well as for the simpler t-J^z ($\alpha=0$) model[35] which has no spin dynamics and has a simple classical Néel ground state. For the t-J model the relative correlation functions are found to be strongly dependent on the momentum

of the quasiparticle, and in good agreement with known results from exact diagonalization.

Furthermore, a detailed investigation of the asymptotic decay of various correlation functions is given. For example, the perturbation of the nearest-neighbor spin-correlation function $C_{\mathbf{R}}$ is found to decay as $1/R^4$ with the distance from the hole. Since the asymptotic behavior of these correlation functions is closely connected with the question of whether $Z_{\mathbf{k}}$ is finite or not, it is important to calculate the deformation of the spin system within the different existing approaches. In the present framework it is found that all perturbations introduced by the hole in the quantum antiferromagnet decay at large distance as power laws with dipolar or more complex angular dependence depending on the momentum of the quasiparticle. Nevertheless this does not lead to a vanishing quasiparticle spectral weight, consistent with earlier numerical results based on the study of the polaron Green's function within the SCBA.[10]

The plan of the paper is as follows: In Secs. II and III, we briefly summarize the self-consistent Born treatment for the Green's function and wave function of the quasiparticle, and provide the framework to calculate expectation values with respect to Reiter's wave function. Section IV deals with the quasiparticle spectral weight and the magnon distribution function, and provides a discussion of the convergence of the approach. The more complex RCF's are studied in Sec. V for two generic cases, the t-J and t-J^z models, i.e., one with spin dynamics and the other without. This section also contains a discussion of the asymptotic behavior of the different correlation functions. The paper concludes with a summary in Sec. VI.

II. SLAVE FERMION APPROACH

In a first step of the reformulation of the problem, holes are described as spinless (slave) fermion operators; i.e., on the A sublattice a spinless fermion creation operator is defined as $h_i^+=c_{i\uparrow}$ while the corresponding operator $c_{i\downarrow}=h_i^+S_i^+$ is expressed as a composite operator, and similarly for the B sublattice.[10] The kinetic energy then consists of terms of the form $-th_ih_j^+S_j^-$, that is, each hop of the fermion is connected with a spin flip. The spin dynamics is described within linear spin-wave (LSW) theory, which provides a satisfactory approximation for the 2D spin-$\frac{1}{2}$ Heisenberg antiferromagnet.

Here we follow Refs. 8–10 and 36, and express spin operators via the Holstein-Primakoff transformation, and simplify the notation by performing a 180° rotation of the spins on the B sublattice,

$$S_i^+ = \tfrac{1}{2}(1+e^{i\mathbf{Q}\cdot\mathbf{R}_i})(2S-a_i^\dagger a_i)^{1/2}a_i$$
$$+ \tfrac{1}{2}(1-e^{i\mathbf{Q}\cdot\mathbf{R}_i})a_i^\dagger(2S-a_i^\dagger a_i)^{1/2}=(S_i^-)^\dagger, \quad (2)$$

$$S_i^z = e^{i\mathbf{Q}\cdot\mathbf{R}_i}(S-a_i^\dagger a_i).$$

Here the origin $\mathbf{R}_0=0$ belongs to A sublattice (spin up) and $\mathbf{Q}=(\pi/a,\pi/a)$. The lattice constant is $a\equiv1$. The spin interaction term is further diagonalized after linearizing spin operators and performing the Bogoliubov transformation

$$\begin{pmatrix} \alpha_{-\mathbf{q}} \\ \alpha_{\mathbf{q}}^{\dagger} \end{pmatrix} = \begin{pmatrix} u_{\mathbf{q}} & -v_{\mathbf{q}} \\ -v_{\mathbf{q}} & u_{\mathbf{q}} \end{pmatrix} \begin{pmatrix} b_{-\mathbf{q}} \\ b_{\mathbf{q}}^{\dagger} \end{pmatrix}, \qquad (3)$$

where $b_{\mathbf{q}}^{\dagger} = N^{-1/2} \Sigma_i e^{-i\mathbf{q}\cdot\mathbf{R}_i} a_i^{\dagger}$, and N is the number of lattice sites. Here we use the usual Bogoliubov coefficients $u_{\mathbf{q}}$ and $v_{\mathbf{q}}$, and the spin-wave dispersion is $\omega_{\mathbf{q}} = 2J\sqrt{1-(\alpha\gamma_{\mathbf{q}})^2}$ with $\gamma_{\mathbf{q}} = (\cos q_x + \cos q_y)/2$. After fermion operators are decoupled into slave fermions and bosons,

$$\widetilde{c}_{i\downarrow} = \tfrac{1}{2}(1+e^{i\mathbf{Q}\cdot\mathbf{R}_i})h_i^{\dagger} + \tfrac{1}{2}(1-e^{i\mathbf{Q}\cdot\mathbf{R}_i})h_i^{\dagger}S_i^{-},$$

$$\widetilde{c}_{i\uparrow} = \tfrac{1}{2}(1+e^{i\mathbf{Q}\cdot\mathbf{R}_i})h_i^{\dagger}S_i^{-} + \tfrac{1}{2}(1-e^{i\mathbf{Q}\cdot\mathbf{R}_i})h_i^{\dagger}, \qquad (4)$$

the fermion-magnon Hamiltonian emerges:[8]

$$H = \frac{1}{\sqrt{N}} \sum_{\mathbf{kq}} (M_{\mathbf{kq}} h_{\mathbf{k}-\mathbf{q}}^{\dagger} h_{\mathbf{k}} \alpha_{\mathbf{q}}^{\dagger} + \text{H.c.}) + \sum_{\mathbf{q}} \omega_{\mathbf{q}} \alpha_{\mathbf{q}}^{\dagger} \alpha_{\mathbf{q}}. \quad (5)$$

A constant term irrelevant to the present discussion has been dropped here. One recognizes that the kinetic energy now appears as a fermion-magnon coupling with a coupling function given by $M_{\mathbf{kq}} = 4t(u_{\mathbf{q}}\gamma_{\mathbf{k}-\mathbf{q}} + v_{\mathbf{q}}\gamma_{\mathbf{k}})$. This Hamiltonian is similar to the small polaron model, except that a kinetic-energy term for the spinless fermions is absent. In the case of the cuprate superconductors, where $t > J$, the model is in the intermediate- or strong-coupling regime, and a self-consistent calculation technique must therefore be chosen.

In the following we will use the hole Green's function

$$G_{\mathbf{k}}(\omega) = \frac{1}{\omega - \Sigma_{\mathbf{k}}(\omega)} = \frac{Z_{\mathbf{k}}}{\omega - \epsilon_{\mathbf{k}}} + G_{\mathbf{k}}^{\text{inc}}(\omega), \qquad (6)$$

where the QP band energy $\epsilon_{\mathbf{k}}$ and the pole strength $Z_{\mathbf{k}}$ are related to the fermion self-energy $\Sigma_{\mathbf{k}}(\omega)$ as $\epsilon_{\mathbf{k}} = \Sigma_{\mathbf{k}}(\epsilon_{\mathbf{k}})$ and $Z_{\mathbf{k}}^{-1} = 1 - \partial\Sigma_{\mathbf{k}}(\omega)/\partial\omega|_{\epsilon_{\mathbf{k}}}$, respectively.

We calculate $\Sigma_{\mathbf{k}}(\omega)$ within the self-consistent Born approximation

$$\Sigma_{\mathbf{k}}(\omega) = \frac{1}{N} \sum_{\mathbf{q}} M_{\mathbf{kq}}^2 G_{\mathbf{k}-\mathbf{q}}(\omega - \omega_{\mathbf{q}}). \qquad (7)$$

Such an approximation amounts to a summation of noncrossing diagrams to all orders. The validity of this approach is well established. The QP dispersion and spectral weight calculated within the SCBA (Ref. 10) agree very well with the exact diagonalization results for small clusters.[6] The spectral weight in the limit $N \to \infty$ is finite.[10] In the extreme $J/t \gg 1$ limit,[37] however, this method leads to $Z_{\mathbf{k}} \to 1$, i.e., an overestimation in comparison to 0.82 obtained for $t = 0$ in Ref. 38. The success of the SCBA has roots in the vanishing of low-order vertex corrections as pointed out by several authors for systems where the hole is coupled to an antiferromagnetic (AFM) spin background.[36,10,39]

III. QUASIPARTICLE WAVE FUNCTION

Given the Green's function in the self-consistent Born approximation, it would be interesting to have a wave function of the quasiparticle which corresponds to the pole in Eq. (6) at energy $\epsilon_{\mathbf{k}} = \Sigma_{\mathbf{k}}(\epsilon_{\mathbf{k}})$. The knowledge of this wave function will allow us to calculate in principle all equal-time

correlation functions which define the perturbation of the AFM background around the hole. Here we follow Reiter's[32] original approach closely, and prove in addition that the quasiparticle weight derived from the wave function is consistent with the well-known expression obtained from the Green's function.

The quasiparticle wave function is defined as the eigenstate of H,

$$H|\Psi_{\mathbf{k}}\rangle = \epsilon_{\mathbf{k}}|\Psi_{\mathbf{k}}\rangle, \qquad (8)$$

which gives rise to the quasiparticle peak in the spectral representation for the Green's function,

$$G_{\mathbf{k}}(\omega) = \sum_m \frac{|\langle \Psi_{\mathbf{k}m}|h_{\mathbf{k}}^{+}|0\rangle|^2}{\omega - \epsilon_{\mathbf{k}m}}. \qquad (9)$$

Here $|0\rangle$ represents the vacuum state with respect to fermion and magnon operators, and $|\Psi_{\mathbf{k}m}\rangle$ is an eigenstate of Hamiltonian Eq. (5) with eigenenergy $\epsilon_{\mathbf{k}m}$. The spectral weight of the quasiparticle state $|\Psi_{\mathbf{k}}\rangle$,

$$Z_{\mathbf{k}} = |\langle \Psi_{\mathbf{k}}|h_{\mathbf{k}}^{\dagger}|0\rangle|^2, \qquad (10)$$

can be quite small; however, it should not scale to zero in the thermodynamic limit, whereas the matrix elements contributing to the incoherent part are of $O(1/N)$ or smaller.

Given the Hamiltonian Eq. (5), we expect the quasiparticle wave function $|\Psi_{\mathbf{k}}\rangle$ to have the form

$$|\Psi_{\mathbf{k}}\rangle = a^0(\mathbf{k})h_{\mathbf{k}}^{+}|0\rangle + \frac{1}{\sqrt{N}} \sum_{\mathbf{q}_1} a^1(\mathbf{k},\mathbf{q}_1)h_{\mathbf{k}-\mathbf{q}_1}^{\dagger} \alpha_{\mathbf{q}_1}^{\dagger}|0\rangle$$

$$+ \frac{1}{N} \sum_{\mathbf{q}_1 \mathbf{q}_2} a^2(\mathbf{k},\mathbf{q}_1,\mathbf{q}_2)h_{\mathbf{k}-\mathbf{q}_1-\mathbf{q}_2}^{\dagger} \alpha_{\mathbf{q}_2}^{\dagger} \alpha_{\mathbf{q}_1}^{\dagger}|0\rangle + \cdots,$$

$$(11)$$

where the coefficients $a^n(\mathbf{k},\mathbf{q}_1,\ldots,\mathbf{q}_n)$ are to be determined.

From the Schrödinger equation we obtain the following system of equations for the expansion coefficients:

$$\omega a^0(\mathbf{k}) - \frac{1}{N} \sum_{\mathbf{q}_1} a^1(\mathbf{k},\mathbf{q}_1)M_{\mathbf{kq}_1} = 0 \qquad (12)$$

and

$$(\omega - \omega_{\mathbf{q}_1})a^1(\mathbf{k},\mathbf{q}_1) - a^0(\mathbf{k})M_{\mathbf{k},\mathbf{q}_1}$$

$$- \frac{1}{N} \sum_{\mathbf{q}_2} a^2(\mathbf{k},\mathbf{q}_1,\mathbf{q}_2)M_{\mathbf{k}-\mathbf{q}_1,\mathbf{q}_2} = 0. \qquad (13)$$

To obtain these equations which correspond to the noncrossing approximation for the Green's function, one has to adopt the following contraction rule: When one magnon is annihilated in the n-magnon component of the wave function [Eq. (11)], only the contribution is considered, where the last magnon in the sequence, i.e., $\alpha_{\mathbf{q}_n}^{\dagger}$, is annihilated. This is reminiscent of the retraceable path approximation in momentum space. The general equation for $n > 0$ reads

$$(\omega - \omega_{\mathbf{q}_1} \cdots - \omega_{\mathbf{q}_n}) a^n(\mathbf{k}, \ldots, \mathbf{q}_n)$$

$$-a^{n-1}(\mathbf{k}, \ldots, \mathbf{q}_n) M_{\mathbf{k}_{n-1}, \mathbf{q}_n}$$

$$-\frac{1}{N} \sum_{\mathbf{q}_{n+1}} a^{n+1}(\mathbf{k}, \ldots, \mathbf{q}_{n+1}) M_{\mathbf{k}_n, \mathbf{q}_{n+1}} = 0,$$

$$(14)$$

where $\mathbf{k}_n = \mathbf{k} - \mathbf{q}_1 - \cdots - \mathbf{q}_n$.

As first shown by Reiter,[32] this sequence of equations (12)–(14) has the general solution

$$a^{n+1}(\mathbf{k}, \ldots, \mathbf{q}_{n+1}) = a^n(\mathbf{k}, \ldots, \mathbf{q}_n) g_{\mathbf{k}_n, \mathbf{q}_{n+1}}, \quad (15)$$

where we introduced the abbreviation

$$g_{\mathbf{k}_n, \mathbf{q}_{n+1}} = M_{\mathbf{k}_n, \mathbf{q}_{n+1}} G_{\mathbf{k}_{n+1}}(\omega - \omega_{\mathbf{q}_1} - \cdots - \omega_{\mathbf{q}_{n+1}}).$$

$$(16)$$

Substituting Eq. (15) into the last term on the left-hand side of Eq. (14), we recognize that this term is identical to the expression Eq. (7) for the self-energy $\Sigma_{\mathbf{k}}(\omega)$ times a^n. For Eq. (14), this yields

$$[\omega - \cdots - \omega_{\mathbf{q}_n} - \Sigma_{\mathbf{k}_n}(\omega - \cdots - \omega_{\mathbf{q}_n})] a^n(\mathbf{k}, \ldots, \mathbf{q}_n)$$

$$-a^{n-1}(\mathbf{k}, \ldots, \mathbf{q}_{n-1}) M_{\mathbf{k}_{n-1}, \mathbf{q}_n} = 0. \quad (17)$$

Since the prefactor of a^n is the inverse of the Green's function $G_{\mathbf{k}_n}(\omega - \omega_{\mathbf{q}_1} - \cdots - \omega_{\mathbf{q}_n})$, this equation is identical to Eq. (15), with n replaced by $n-1$. It only remains to be shown that Eq. (12) also is solved. Equation (12) becomes

$$a^0(\mathbf{k})[\omega - \Sigma_{\mathbf{k}}(\omega)] = 0, \quad (18)$$

which has a nontrivial solution $a^0(\mathbf{k}) \neq 0$ at the QP energy $\omega = \epsilon_{\mathbf{k}}$. The knowledge of the Green's function Eq. (6) is sufficient to calculate from Eq. (15) iteratively the coefficients $a^n(\mathbf{k}, \mathbf{q}_1, \ldots, \mathbf{q}_n)$.

The coefficient $a^0(\mathbf{k})$ which determines the QP weight $Z_{\mathbf{k}} = [a^0(\mathbf{k})]^2$ follows from the normalization of the wave function $\langle \Psi_{\mathbf{k}} | \Psi_{\mathbf{k}} \rangle = \Sigma_{n=0}^{\infty} |a^n(\mathbf{k}, \ldots, \mathbf{q}_n)|^2 = 1$,

$$\langle \Psi_{\mathbf{k}} | \Psi_{\mathbf{k}} \rangle = [a^0(\mathbf{k})]^2 \left\{ 1 + \frac{1}{N} \sum_{\mathbf{q}_1} g_{\mathbf{k}, \mathbf{q}_1}^2 \right.$$

$$\left. + \frac{1}{N^2} \sum_{\mathbf{q}_1 \mathbf{q}_2} g_{\mathbf{k}, \mathbf{q}_1}^2 g_{\mathbf{k}-\mathbf{q}_1, \mathbf{q}_2}^2 + \cdots \right\}. \quad (19)$$

When one calculates the derivative $\partial \Sigma_{\mathbf{k}}(\omega)/\partial \omega$ from Eq. (7), and compares the result with Eq. (19), it is easy to see that[20]

$$\langle \Psi_{\mathbf{k}} | \Psi_{\mathbf{k}} \rangle = [a^0(\mathbf{k})]^2 \left(1 - \frac{\partial \Sigma_k(\omega)}{\partial \omega} \right) \bigg|_{\omega = \epsilon_k}. \quad (20)$$

As $|\Psi_{\mathbf{k}}\rangle$ is normalized to 1, $[a^0(\mathbf{k})]^2$ is indeed identical to the QP spectral weight as calculated directly from G. This latter step is important, since it accomplishes the proof of the internal consistency of G and Ψ, i.e., where both are calculated within the self-consistent Born approximation. It
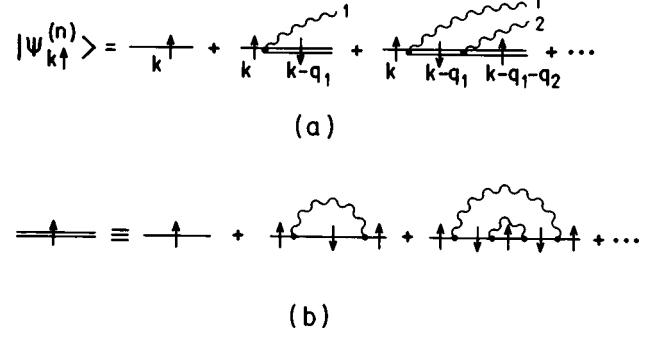

(a)

(b)

FIG. 1. Diagrammatic representation of the wave function $|\Psi_{\mathbf{k}\tau}^{(n)}\rangle$ for $\tau = \uparrow$. (a) The first three terms contain no-magnon, one-magnon, and two-magnon excitations, respectively. (b) The double line represents the single-particle Green's function in the noncrossing approximation.

should be emphasized that the above derivation does not rely on the assumption that the coupling term in the Hamiltonian is small.

Because of the presence of AFM long-range order, the quasiparticles move on one sublattice, while visiting the other sublattice only virtually. In view of the "degeneracies" $\epsilon_{\mathbf{k}+\mathbf{Q}} = \epsilon_{\mathbf{k}}$ and $G_{\mathbf{k}+\mathbf{Q}} = G_{\mathbf{k}}$, we define Bloch operators

$$h_{\mathbf{k}\tau}^{\dagger} = 2^{-1/2}(h_{\mathbf{k}}^{\dagger} + \tau h_{\mathbf{k}+\mathbf{Q}}^{\dagger}), \quad (21)$$

which create holes on the $\uparrow$ ($\downarrow$) sublattice for $\tau = 1(-1)$, respectively. The momenta $\mathbf{k}$ are now restricted to the reduced (AFM) Brillouin zone. The corresponding wave functions including magnon operators up to order n, are

$$|\Psi_{\mathbf{k}\tau}^{(n)}\rangle = \frac{1}{\sqrt{2}} (|\Psi_{\mathbf{k}}^{(n)}\rangle + \tau |\Psi_{\mathbf{k}+\mathbf{Q}}^{(n)}\rangle), \quad (22)$$

with $|\Psi_{\mathbf{k}}^{(n)}\rangle$ following from Eq. (11):

$$|\Psi_{\mathbf{k}}^{(n)}\rangle = Z_{\mathbf{k}}^{1/2} \left[h_{\mathbf{k}}^{\dagger} + N^{-1/2} \sum_{\mathbf{q}_1} g_{\mathbf{k}, \mathbf{q}_1} h_{\mathbf{k}_1}^{\dagger} \alpha_{\mathbf{q}_1}^{\dagger} \right.$$

$$+ \cdots + N^{-n/2} \sum_{\mathbf{q}_1, \ldots, \mathbf{q}_n} g_{\mathbf{k}, \mathbf{q}_1} g_{\mathbf{k}-\mathbf{q}_1, \mathbf{q}_2} \cdots$$

$$\left. \times g_{\mathbf{k}-\mathbf{q}_1-\cdots-\mathbf{q}_{n-1}, \mathbf{q}_n} h_{\mathbf{k}-\mathbf{q}_1-\cdots-\mathbf{q}_n}^{\dagger} \alpha_{\mathbf{q}_1}^{\dagger} \cdots \alpha_{\mathbf{q}_n}^{\dagger} \right] |0\rangle.$$

$$(23)$$

Here $g_{\mathbf{k}, \mathbf{q}} = M_{\mathbf{k}\mathbf{q}} G_{\mathbf{k}-\mathbf{q}}(\epsilon_{\mathbf{k}} - \omega_{\mathbf{q}})$, as defined in Eq. (16). We note that the Green's function G in $g_{\mathbf{k}, \mathbf{q}}$ is always evaluated below the lowest pole and are therefore real. For example, in $G_{\mathbf{k}-\mathbf{q}}(\epsilon_{\mathbf{k}} - \omega_{\mathbf{q}})$ the energy $\epsilon_{\mathbf{k}-\mathbf{q}} > \epsilon_{\mathbf{k}} - \omega_{\mathbf{q}}$, hence $g_{\mathbf{k}, \mathbf{q}}$ is real. This is actually a subtle consequence of the self-consistent evaluation of the Green's function which leads to a smaller energy variation of the QP energy compared to the spin-wave dispersion.[10] We stress that this also holds true in the strong-coupling case, where the $\epsilon_{\mathbf{k}}$ variation is also of order J, i.e., comparable with spin-wave energies. The choice of sublattice wave functions Eq. (22) is convenient, since they are eigenstates of S_{tot}^z with eigenvalues $\pm \frac{1}{2}$.

The diagrammatic structure of the wave function $|\Psi_{\mathbf{k}\uparrow}^{(n)}\rangle$ is shown in Fig. 1(a). The translation rules are straightforward:
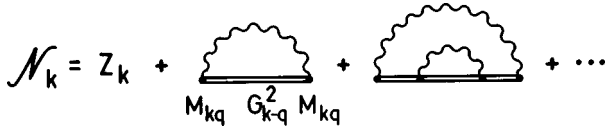
FIG. 2. Diagrammatic representation of the norm $\mathcal{N}_\mathbf{k}$. The first term—containing no magnon line—is identical to the QP pole strength $Z_\mathbf{k}$.

(1) Open ends on the right correspond to operators $h^\dagger_{\mathbf{k}-\mathbf{q}_1-\cdots-\mathbf{q}_n}$ and $\alpha^\dagger_{\mathbf{q}_1}\cdots\alpha^\dagger_{\mathbf{q}_n}$, (2) thin lines are associated with $\sqrt{Z_\mathbf{k}}$, (3) a vertex (dot) connected with a double line corresponds to $g_{\mathbf{k},\mathbf{q}}$, and (4) there is a momentum sum for each magnon line. It is obvious that the wave function does not correspond to a strict order n expansion with respect to the fermion-magnon coupling, since the Green's function [Fig. 1(b)], is already evaluated self-consistently with respect to this interaction. In Sec. IV we will investigate the relative importance of the different terms in the wave function Eq. (23), and address the question under which conditions this series can be truncated.

IV. MAGNON DISTRIBUTION FUNCTION

The first question one may ask is the following: "How many magnons are involved in the formation of the polaron?" As the coupling between hole and spin excitations is the kinetic energy of the t-J model, small values of J/t correspond to strong coupling (small spin stiffness), where many magnons are excited by the hole motion. In order to estimate the number n of magnon terms needed in the wave function, we calculated the norm $\mathcal{N}_\mathbf{k}$,

$$\mathcal{N}_\mathbf{k} = \langle \Psi^{(n)}_{\mathbf{k}\tau} | \Psi^{(n)}_{\mathbf{k}\tau} \rangle = \sum_{m=0}^{n} A^{(m)}_\mathbf{k}. \tag{24}$$

The distribution function $A^{(m)}_\mathbf{k}$ defines the probability for the n-magnon contribution in the wave function. A similar study on a small cluster was presented in Ref. 40.

In Fig. 2 the norm is presented diagrammatically consistent with Eq. (19). Each term $A^{(m)}_\mathbf{k}$ corresponds to a single noncrossing diagram with n magnons. Vertices denoted with dots correspond to the fermion-magnon coupling matrix elements $M_{\mathbf{kq}}$ and the double line to the *square* of Green's function Eq. (6) calculated within SCBA. The analytical expression for $A^{(m)}_\mathbf{k}$ is independent of τ, and given by

$$A^{(m)}_\mathbf{k} = \frac{Z_\mathbf{k}}{N^m} \sum_{\mathbf{q}_1,\ldots,\mathbf{q}_m} g^2_{\mathbf{k},\mathbf{q}_1} g^2_{\mathbf{k}-\mathbf{q}_1,\mathbf{q}_2} \cdots g^2_{\mathbf{k}-\mathbf{q}_1-\cdots,\mathbf{q}_m} \tag{25}$$

for $m>0$, while $A^{(0)}_\mathbf{k} = Z_\mathbf{k}$. From Eq. (19) we know that $\mathcal{N}_\mathbf{k} \to 1$ in the limit $n \to \infty$. This normalization condition will serve as a check of our numerical procedure.

It is instructive to study the distribution function $A^{(m)}_\mathbf{k}$ first in the case of the the t-J^z model ($\alpha=0$). In this limit of model Eq. (1) the analysis becomes simple because there is no intrinsic spin dynamics. The SCBA equations for the self-energy are independent of $\mathbf{k}$, and reduce to one equation $\Sigma_\mathbf{k}(\omega) = 4t^2[\omega - 2J^z - \Sigma_\mathbf{k}(\omega-2J^z)]^{-1}$.[9] Equation (25) can then be expressed in a recurrence form
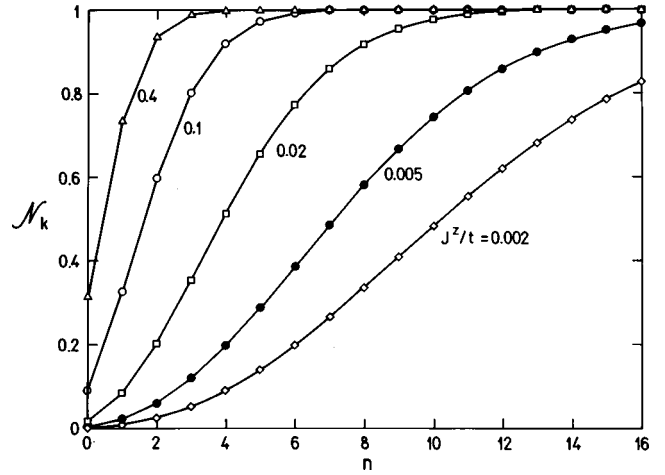

FIG. 3. The norm $\mathcal{N}_\mathbf{k}$ in the Ising limit as a function of the number n of magnons included in the wave function for various J^z/t.

$$A^{(m+1)}_\mathbf{k} = A^{(m)}_\mathbf{k}[2tG_\mathbf{k}(\epsilon_\mathbf{k} - 2mJ^z)]^2. \tag{26}$$

The norm $\mathcal{N}_\mathbf{k}$ is shown in Fig. 3 as a function of the number of magnon terms n for various J^z/t. A crossover between the weak- and strong-coupling regimes occurs at $J^z/t \sim 0.3$. For smaller J^z/t the number of magnon terms needed to fulfill the sum rule $\mathcal{N}_\mathbf{k} = 1$ increases rapidly. In Fig. 4 the distribution of magnons $A^{(m)}_\mathbf{k}$ is displayed for the strong-coupling case, $J^z/t \ll 1$. In this regime $A^{(m)}_\mathbf{k}$ has a maximum at a finite value n, which increases with the coupling constant t/J^z.

The average number of magnons forming the spin polaron may be defined as

$$\langle n \rangle = \langle \Psi^{(n)}_{\mathbf{k}\tau} | \sum_\mathbf{q} \alpha^\dagger_\mathbf{q}\alpha_\mathbf{q} | \Psi^{(n)}_{\mathbf{k}\tau} \rangle = \sum_m m A^{(m)}_\mathbf{k}. \tag{27}$$

In the Ising limit, $\langle n \rangle$ is identical to the average number of spin deviations (local magnons) $\langle \Sigma_i S^+_i S^-_i \rangle = \langle \Sigma_i a^\dagger_i a_i \rangle$. It is evident that the latter expression is proportional to the average string length l_{av} (Ref. 19) of overturned spins in the Néel state created by the hole motion. As the string potential is an approximately linear function of the string length, this im-
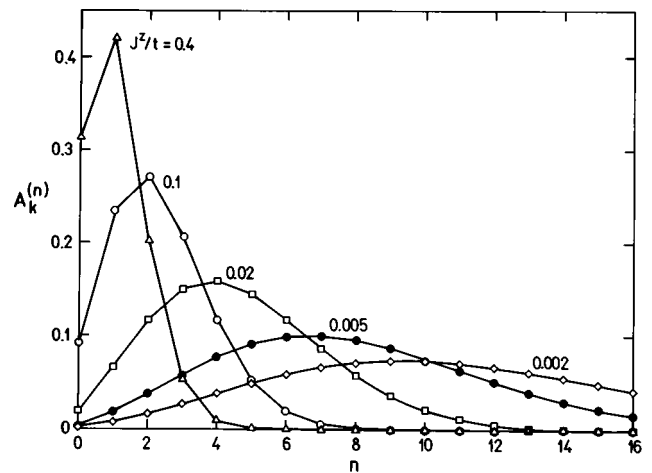

FIG. 4. The distribution of the number of magnons $A^{(n)}_\mathbf{k}$ as a function of n for various J^z/t.
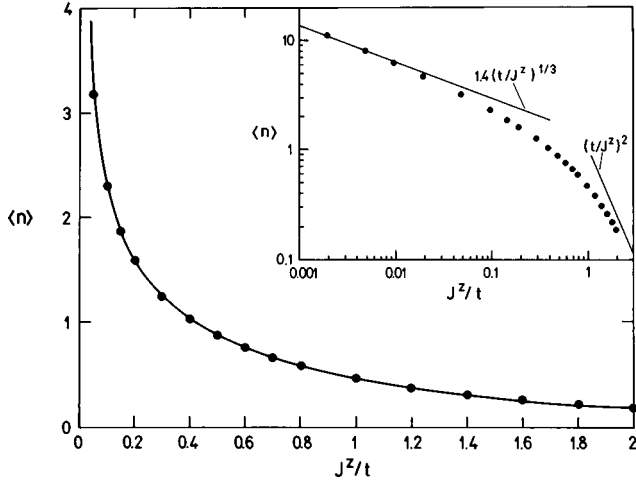
FIG. 5. Average number of magnons $\langle n \rangle$ in the Ising limit as a function of J^z/t. The inset shows $\langle n \rangle$ on a logarithmic scale compared with asymptotic results.

plies $\langle n \rangle \propto l_{\mathrm{av}} \propto (t/J^z)^{1/3}$. This estimate is reasonable for long strings, i.e., small J^z/t. In Fig. 5 we present $\langle n \rangle$ as a function of J^z/t calculated with up to 40 magnon terms in the wave function. For large $J^z/t \gg 1$ only the leading term $m=1$ in Eq. (27) is relevant, therefore the asymptotic result is $\langle n \rangle = (t/J^z)^2$. For $J^z/t \ll 1$ we find excellent agreement with the result $\langle n \rangle = 1.4 (t/J^z)^{1/3}$ obtained by Mattis and Chen.[41]

From these results for the t-J^z model it is clear for $J^z/t \gtrsim 0.4$ the wave function can be truncated at $n=3$ or even at $n=2$. We note that the same holds true for the t-J model.[20]

In Figs. 6(a) and 6(b) the numerical results for the norm $\mathcal{N}_{\mathbf{k}}$ of the t-J model are shown for $\mathbf{k}=0$ and $\mathbf{k}=(\pi/2, \pi/2)$, respectively, both calculated with up to $n=3$ magnons kept in the wave function. For $J=0.4$, three-magnon contributions are necessary to fulfill the norm. The quasiparticle spectral weight $Z_{\mathbf{k}}$, which corresponds to the $n=0$ term displayed in Figs. 6(a) and 6(b), is always finite except in the limit of vanishing spin stiffness $J=0$. Thus our wave function does not lead to an orthogonality catastrophe. This result will be further complemented in Sec. V by a detailed study of the asymptotic decay of the spin-polaron correlation functions.

The question whether the QP spectral weight $Z_{\mathbf{k}}$ for the t-J model is finite or not is still not completely settled. Numerical results obtained on small clusters are in a good agreement with the results obtained from the SCBA Eqs. (7).[10] In the SCBA formalism Eq. (5), $Z_{\mathbf{k}}$ is finite,[9,36,10] because the hole-magnon coupling matrix element for $q \to 0$ is not singular, and therefore the hole is weakly coupled to low-energy spin waves. In Ref. 28 it was argued that $Z_{\mathbf{k}}$ should vanish nevertheless, because of stringlike phases associated with the hole motion (due to hidden Marshall signs). We stress that the Marshall sign convention is implicitly included in our present formulation. In fact, the vacuum state $|0\rangle$ (originating via unitary transformation) is equivalent to the quantum Néel ground state of the $T=0$ Heisenberg model, and thus by construction obeys the Marshall sign rule in the original basis, i.e., before the $180°$ rotation of the B sublattice. After the transformation Eq. (2), there are no additional phases in the transformed Hamiltonian due to the Marshall sign.
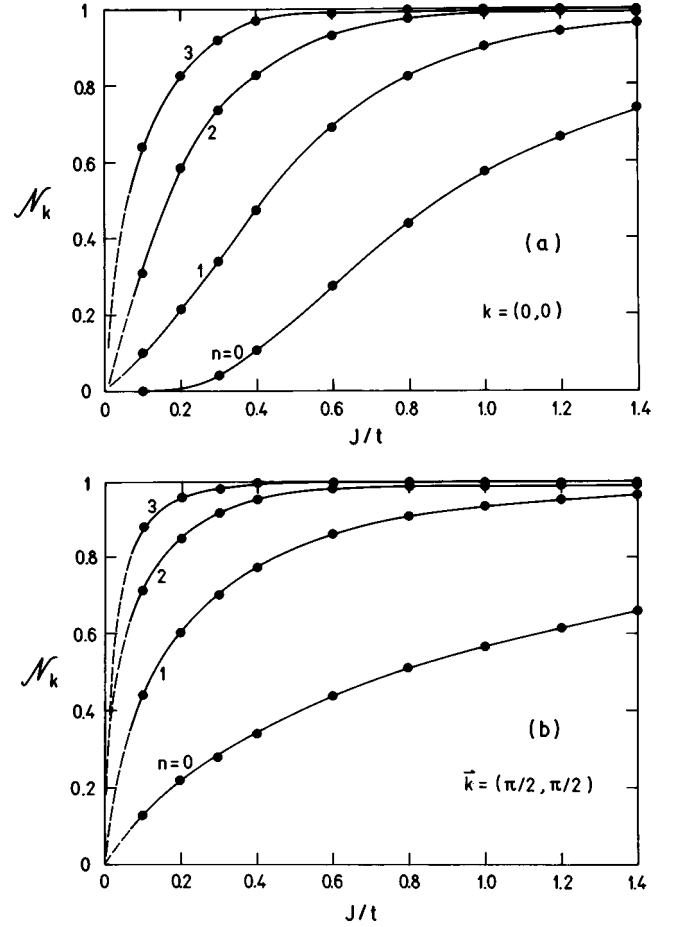

FIG. 6. The norm $\mathcal{N}_{\mathbf{k}}$ for the t-J model as a function of J/t including magnons up to order $n=3$ in the quasiparticle wave function. (a) Momentum at the top of the QP band at $\mathbf{k}=0$, and (b) at $\mathbf{k}=(3\pi/8, 3\pi/8)$, i.e., close to the QP-band minimum. The numerical calculation was performed for a momentum-space grid corresponding to a 32×32 system. The solid and dashed lines are guides to the eye only.

Not considered in the present treatment, is the effect of the four broken bonds meeting at the site of the hole. This leads to an additional relaxation of the spin correlations, and hence to a reduction of the quasiparticle weight. This effect is expected to be strongest in the limit $t=0$. The exact result for the spectral weight in this case is $Z=0.82$, and was derived by Mal'shukov and Mahan[38] (as compared to 1 in the present treatment). The energy change due to the broken bonds must also be included in the Born approximation if one wants to compare the quasiparticle energies with those from exact diagonalization, as discussed by Martínez and Horsch.[10]

V. SPIN-POLARON CORRELATION FUNCTIONS

The spatial structure of the spin polaron can be described with various correlation functions measuring the perturbation of the spin system relative to the position of the moving hole. As we shall see, these correlation functions are strikingly different in the t-J and the t-J^z models—a consequence of the absence of spin dynamics in the latter model. In the t-J model perturbations created by the hole are carried away by spin waves thereby generating a power-law perturbation pat-
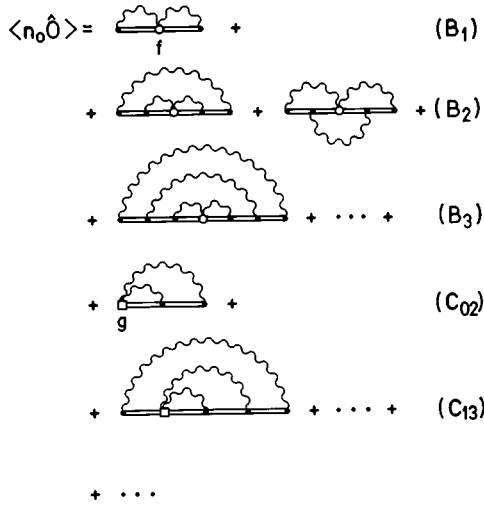
FIG. 7. Diagrammatic representation of correlation functions. Each class of (B_n) diagrams contains n noncrossing diagrams. (C_{nm}) diagrams appear always in pairs with the H.c. counterparts. For a detailed description, see the text.

tern with an interesting angular dependence, whereas in the absence of spin dynamics the perturbations are characterized by an isotropic Gaussian decay.

Such relative correlation functions can be evaluated using the quasiparticle wave function. One of the simplest correlation functions is the distribution of magnons around the hole

$$N_{\mathbf{R}} = \langle \Psi_{\mathbf{k}\tau}^{(n)} | \sum_i n_i a_{\mathbf{R}_i+\mathbf{R}}^\dagger a_{\mathbf{R}_i+\mathbf{R}} | \Psi_{\mathbf{k}\tau}^{(n)} \rangle \equiv \langle n_0 (a_{\mathbf{R}}^\dagger a_{\mathbf{R}}) \rangle. \tag{28}$$

Here $n_i = h_i^\dagger h_i$ is density operator for holes at site i with position $\mathbf{R}_i$. $N_{\mathbf{R}}$ also corresponds to the distribution of spin deviations, $\langle n_0 (S_{\mathbf{R}}^+ S_{\mathbf{R}}^-) \rangle$. Therefore it provides a suitable measure of the polaron size. This correlation function is also proportional to the distributions $\langle n_0 (S_{\mathbf{R}}^x)^2 \rangle = \langle n_0 (S_{\mathbf{R}}^y)^2 \rangle$.

Correlation functions such as $N_{\mathbf{R}}$ are evaluated using similar diagrams as in the calculation of the norm $\mathcal{N}_{\mathbf{k}}$. One has to evaluate the expectation values

$$\langle \Psi_{\mathbf{k}\tau}^{(n)} | \sum_i n_i \hat{\mathcal{O}}_{\mathbf{R}_i+\mathbf{R}} | \Psi_{\mathbf{k}\tau}^{(n)} \rangle \equiv \langle n_0 \hat{\mathcal{O}}_{\mathbf{R}} \rangle. \tag{29}$$

Here the summation Σ_i corresponds to all lattice sites, and the density operator for the hole

$$n_i = \frac{1}{N} \sum_{\mathbf{k}_1 \mathbf{k}_2} e^{i(\mathbf{k}_2-\mathbf{k}_1)\cdot\mathbf{R}_i} h_{\mathbf{k}_1}^\dagger h_{\mathbf{k}_2} \tag{30}$$

has to be expressed in terms of operators $h_{\mathbf{k}\tau}$ [Eq. (21)]. The operator $\hat{\mathcal{O}}_{\mathbf{R}}$ is decomposed into magnon variables as

$$\hat{\mathcal{O}}_{\mathbf{R}} = \frac{1}{N} \sum_{\mathbf{q}_1 \mathbf{q}_2} [f_{\mathbf{q}_1 \mathbf{q}_2}(\mathbf{R}) \alpha_{\mathbf{q}_1}^\dagger \alpha_{\mathbf{q}_2} + g_{\mathbf{q}_1 \mathbf{q}_2}(\mathbf{R}) \alpha_{\mathbf{q}_1} \alpha_{\mathbf{q}_2} + \text{H.c.}].$$

The diagrammatic structure of the contributions for a general correlation function of this type is presented in Fig. 7. The first class of diagrams is symmetric and derives from the

vertex function $f_{\mathbf{q}_1 \mathbf{q}_2}(\mathbf{R})$. These diagrams, denoted by (B_n), arise as diagonal contributions from the n-magnon component of the wave function.

The construction rule for these diagrams is the following: If the vertex f (circle) as well as the connected two magnon lines (together with their vertices and associated double lines) are removed from the diagram, one must arrive at a diagram contained in the expression for the norm (Fig. 2). Otherwise the diagram is not consistent with the self-consistent Born approximation, and should be dropped.

The second class of diagrams (C_{nm}) is asymmetric and corresponds to the vertex function $g_{\mathbf{q}_1 \mathbf{q}_2}(\mathbf{R})$ which connects n-magnon contributions with $m=(n\pm2)$-magnon terms in the wave function. Again only such diagrams must be taken into account which are consistent with the construction rule formulated before.

The vertex functions f and g are expressed in terms of Bogoliubov coefficients and thus strongly momentum dependent. For the case of the correlation function $N_{\mathbf{R}}$ we have

$$f_{\mathbf{q}_1 \mathbf{q}_2}(\mathbf{R}) = \tfrac{1}{2}(u_{\mathbf{q}_1} u_{\mathbf{q}_2} + v_{\mathbf{q}_1} v_{\mathbf{q}_2}) e^{i(\mathbf{q}_1-\mathbf{q}_2)\cdot\mathbf{R}},$$

$$g_{\mathbf{q}_1 \mathbf{q}_2}(\mathbf{R}) = \tfrac{1}{2}(u_{\mathbf{q}_1} v_{\mathbf{q}_2} + v_{\mathbf{q}_1} u_{\mathbf{q}_2}) e^{i(\mathbf{q}_1+\mathbf{q}_2)\cdot\mathbf{R}}. \tag{31}$$

In order to illustrate a typical calculation of matrix elements needed in the correlation functions, here we present the second-order contributions B_2 in Fig. 7,

$$B_2 = N^{-3} \sum_{\mathbf{q}_1 \mathbf{q}_2 \mathbf{q}_3} f_{\mathbf{q}_1 \mathbf{q}_2}(\mathbf{R})(g_{\mathbf{k},\mathbf{q}_3} g_{\mathbf{k}-\mathbf{q}_3,\mathbf{q}_1} g_{\mathbf{k}-\mathbf{q}_3,\mathbf{q}_2} g_{\mathbf{k},\mathbf{q}_3}$$

$$+ g_{\mathbf{k},\mathbf{q}_1} g_{\mathbf{k}-\mathbf{q}_1,\mathbf{q}_3} g_{\mathbf{k}-\mathbf{q}_2,\mathbf{q}_3} g_{\mathbf{k},\mathbf{q}_2}), \tag{32}$$

where the first and second terms correspond to noncrossing and crossing terms, respectively.

A. Ising limit ($\alpha = 0$)

In general, correlation functions and the corresponding matrix elements have to be evaluated numerically, which is easy for a not-too-large n up to ~ 5. The t-J^z model is an exception, since the Bogoliubov factors simplify to $u_{\mathbf{q}} = 1$ and $v_{\mathbf{q}} = 0$. Thus $\text{Re} f_{\mathbf{q}_1 \mathbf{q}_2}(\mathbf{R}) = \cos((\mathbf{q}_1-\mathbf{q}_2)\cdot\mathbf{R})$ and $g_{\mathbf{q}_1 \mathbf{q}_2}(\mathbf{R}) = 0$, respectively. As the Green's function is dispersionless, it is possible to express the matrix elements analytically and perform the summation of diagrams (B_n) to any order. Furthermore, diagrams (C_{nm}) are zero. It is instructive to express the wave function in real space. Each n-magnon term can then be visualized as a string of n steps with starting point at the origin. From such a study one can gain insight into the noncrossing structure of the wave function and correlation functions.

The SCBA is similar to the retraceable path approximation, yet with the important difference that in SCBA the hole can also hop backwards on its path. At the level of the Green's function the differences were discussed in Ref. 10. The result for the magnon distribution function [Eq. (28)] can therefore be expressed as

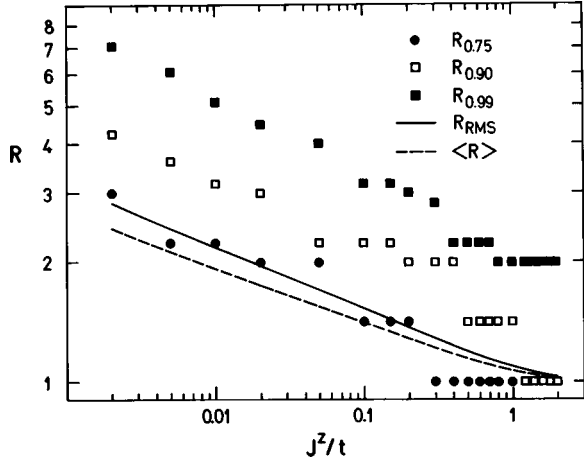$$N_{\mathbf{R}} = \sum_{m=1}^n p_m(\mathbf{R}) P_m, \tag{33}$$

FIG. 8. Radius of the polaron in the Ising limit vs J^z/t for various definitions: R_p for $p=0.75$ (full circles), $p=0.90$ (open squares), and full squares for $p=0.99$. Here p defines the fraction of spin deviations within the radius R_p. The full line represents the root-mean-square radius R_{rms}, while the dashed line gives the average radius $\langle R \rangle$.

where $P_m = \Sigma_{j=m}^n A_{\mathbf{k}}^{(j)}$ can be interpreted as a probability to have at least m local magnons excited. The coefficients $p_m(\mathbf{R})$ represent the probability that a string of m excited local magnons ends at a given lattice position $\mathbf{R}$. This distribution can be determined by counting all possible paths of m steps, where in each step all z neighbors can be reached,

$$ p_m(\mathbf{R}) = 4^{-m} \binom{m}{m_+} \binom{m}{m_-}. \tag{34} $$

Here $m_\pm = (m - ||R_x| \pm |R_y||)/2$ must be a non-negative integer, otherwise $p_m(\mathbf{R}) = 0$. This result is free of boundary conditions.

The correlation function $N_{\mathbf{R}}$ can be used to determine the spatial size of the polaron in the Ising limit. We define the size of the polaron quantitatively by the radius R_p (the element of the Bravais lattice), which encloses a given fraction p of the total number of spin deviations, $p = \langle n \rangle^{-1} \Sigma_{R \le R_p} N_{\mathbf{R}}$. In Fig. 8 the polaron radius R_p vs J/t is shown for three different values of $p = 0.75$, 0.9, and 0.99. In the physically interesting regime $J^z/t \sim 0.3$, the polaron is contained within the radius $R < 2$. The scaling $R_p \propto \langle n \rangle^{1/2} \propto (t/J^z)^{1/6}$ expected for the polaron[19,20] is well established. We have also calculated the average radius, $\langle R \rangle = \langle n \rangle^{-1} \Sigma_{\mathbf{R}} |\mathbf{R}| N_{\mathbf{R}}$, and the root-mean-square radius $R_{\text{rms}} = (\langle n \rangle^{-1} \Sigma_{\mathbf{R}} |\mathbf{R}|^2 N_{\mathbf{R}})^{1/2}$. In Fig. 8 R_{rms} and $\langle R \rangle$ are presented with solid and dashed lines, respectively. The rms radius can be well fitted with $R = 1.06(t/J)^{0.157}$ for $J^z/t < 1$.

In the Ising limit the total spin is not conserved. However, the z component of the spin is a conserved quantity. A state with one static hole ($t=0$) at the site i_0 has by definition the z component of total spin $S_{\text{tot}}^z = \Sigma_{i \ne i_0} S_i^z = -\tau/2$ ($\tau = \pm 1$), i.e., the spin of one site of the sublattice not corresponding to i_0. If the hole becomes mobile ($t \ne 0$), some spins around the hole deviate from the Néel order. The region where the spin order is disturbed corresponds to the spin polaron defined above. The correlation function describing the spatial distribution of spin around the hole is thus
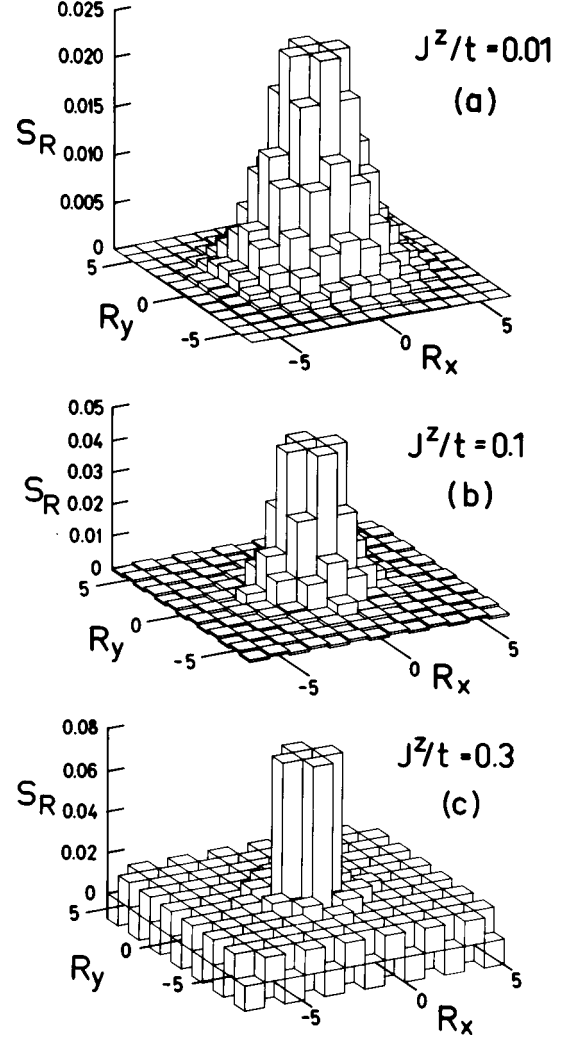

FIG. 9. Distribution of the z component of spin $S_{\mathbf{R}} = \langle n_0 S_{\mathbf{R}}^z \rangle$ around the moving hole for three different values for J^z/t.

$$ S_{\mathbf{R}} = \langle n_0 S_{\mathbf{R}}^z \rangle = \tau e^{i\mathbf{Q}\cdot\mathbf{R}} \sum_i e^{i\mathbf{Q}\cdot\mathbf{R}_i} [\tfrac{1}{2}\langle n_i \rangle - \langle n_i a_{\mathbf{R}_i+\mathbf{R}}^\dagger a_{\mathbf{R}_i+\mathbf{R}} \rangle], \tag{35} $$

where we have expressed spin operators in terms of magnons according to Eq. (2). The conservation of spin corresponds to the sum rule $\Sigma_{R \ne 0} S_{\mathbf{R}} = -\tau/2$. The local spin operator is, within the LSW approximation, related to the number of bosons, $S_i^z = \tfrac{1}{2} - a_i^\dagger a_i$. However, $S_{\mathbf{R}}$ is due to the factor $\exp(i\mathbf{Q}\cdot\mathbf{R}_i)$ nontrivially related to $N_{\mathbf{R}}$, and has to be calculated independently. After carrying out steps similar to those in the evaluation of $N_{\mathbf{R}}$, one obtains

$$ S_{\mathbf{R}} = \tau e^{i\mathbf{Q}\cdot\mathbf{R}} \left[\tfrac{1}{2} \widetilde{P}_0 - \sum_{m=1}^n p_m(\mathbf{R}) \widetilde{P}_m \right], \tag{36} $$

and $\widetilde{P}_m = \Sigma_{j=m}^n (-1)^j A_{\mathbf{k}}^{(j)}$.

The spin-correlation function $S_{\mathbf{R}}$ for several J^z/t values is given in Fig. 9. We performed the calculation for n up to 40, which was more than sufficient to obtain converged values. The results can be qualitatively understood visualizing the correlation function $S_{\mathbf{R}}$ in the moving coordinate frame of
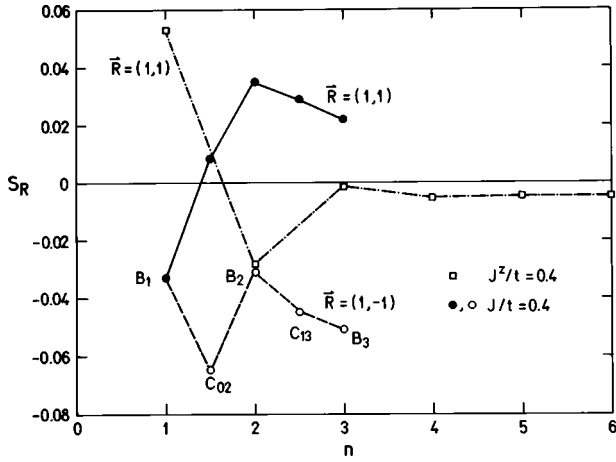
FIG. 10. The dependence of $S_\mathbf{R}$ on the number of magnon terms n in the wave function. In the Ising limit $S_{(1,1)}$ (dash-dotted line) is essentially converged for $n>3$, given $J^z/t=0.4$. In the Heisenberg case the contributions from different diagrams to $S_\mathbf{R}$ are shown for $\mathbf{R}=(1,1)$ (solid) and $\mathbf{R}=(1,-1)$ (dashed line), respectively, for $J/t=0.4$ and $\mathbf{k}=(\pi/2,\pi/2)$. For the classification of diagrams (B_n) and (C_{nm}) see Fig. 7.

the hole. For large J^z/t the hole moves slowly through the Néel-ordered background, and on the average spends more time on sublattice τ. The alternating contribution to $S_\mathbf{R}$ corresponds to the AFM-ordered background, and is given by the first term on the right-hand side of Eq. (35), which is apart from the AFM alternation independent of $\mathbf{R}$. It represents the difference in the probability that the hole sits on the $\uparrow$ and $\downarrow$ sublattices, respectively. This background contribution tends to zero for $J^z/t \ll 1$, where the hole rapidly hops from one sublattice to the other. The second term in $S_\mathbf{R}$ carries all spatial dependence, i.e., defines the region of spin disturbance, and becomes dominant at $J^z/t \ll 1$.

We would like to stress here that the disappearance of the staggered Néel structure for small J^z/t in this correlation function is simply a consequence of the fact that the hole visits the two sublattices with equal probability, and it does not mean that the antiferromagnetic order is no longer present as one could naively conclude from similar results of a finite cluster diagonalization. We note that our results resemble surprisingly well the results for $S_\mathbf{R}$ obtained in exact diagonalization studies for small clusters.[3,4]

In Fig. 10 we show with open squares the dependence of $S_\mathbf{R}$ at $\mathbf{R}=(1,1)$ with $J^z/t=0.4$ on the number of magnons n taken into account in the calculation. The results for other J^z/t values are in agreement with the results for $\mathcal{N}_\mathbf{k}$, where we found that above (below) $J^z/t \sim 0.3$ a relatively small (large) number of magnons are excited and therefore needed in the evaluation of the correlation functions.

The conservation of the total spin z component can be tested by summing up $\Sigma_{R \neq 0} S_\mathbf{R}$. The total spin S_{tot}^z is presented in Fig. 11 as a function of J^z/t with diamonds, and the full line is a guide to the eye. S_{tot}^z consists of two parts. The first corresponds to the first term in Eq. (36), $\frac{1}{2}\widetilde{P}_0$, and is shown with the dashed curve. $\widetilde{P}_0$ represents the difference in the probability of the hole sitting on sublattice $\uparrow$ or $\downarrow$. The second term in Eq. (36) is not presented separately. The interchange of importance of the two contributions is in agree-
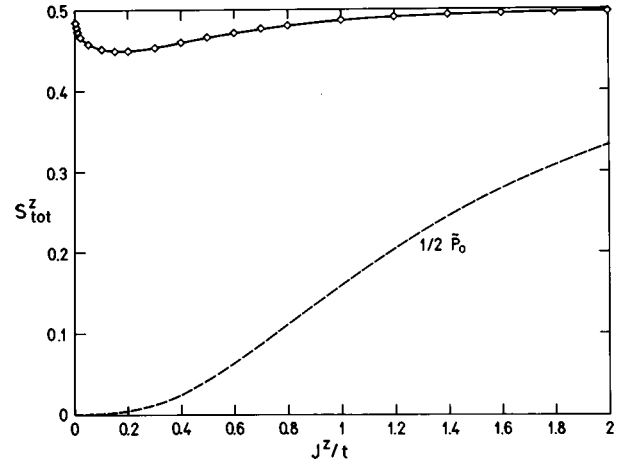

FIG. 11. The total z component of spin S_{tot}^z vs J^z/t (diamonds). The dashed line represents $\frac{1}{2}\widetilde{P}_0$ in Eq. (36), where $\widetilde{P}_0$ is the difference of the probabilities for the hole to occupy sublattice $\uparrow$ or $\downarrow$, respectively.

ment with the discussion above. The small violation of the S_{tot}^z conservation law is a consequence of the Holstein-Primakoff representation of spin operators. We also calculated S_{tot}^z as a function of n. For $J^z/t>0.3$ only three magnon terms included in the wave function give sufficient accuracy in agreement with calculation of the norm $\mathcal{N}_\mathbf{k}$.

B. Heisenberg limit ($\alpha=1$)

The important features of the t-J model are the following: (i) The spin dynamics described by antiferromagnetic spin waves, which have a linear dispersion around $q=(0,0)$ and (π,π), respectively. (ii) The ground state of the model in two-dimensions is a quantum Néel state, i.e., more complex than the simple classical Néel ground state of the t-J^z model. An immediate consequence of (i) is that a spin deviation which is created by a single move of the hole will propagate away from the hole in form of a spin wave, until it is reabsorbed at a later instance. The long-wavelength spin excitations determine the distortion of the quantum antiferromagnet at large distances from the hole.

A further aim of our study of RCF's is to show that the spin correlations remain antiferromagnetic in the vicinity of the hole. The antiferromagnetic correlations are weakened yet not ferromagnetic. The ferromagnetic polaron picture, i.e., a carrier accompanied by a ferromagnetically aligned spin cluster, does not apply here. Ferromagnetic polarons are a quite popular scenario usually inferred by a generalization of Nagaoka's theorem,[42] which applies to the $J=0$ model, to finite exchange interaction J.

To gain more insight into the complex angular dependence of the relative correlation functions, in addition to the numerical results (which include up to $n=3$ magnons) we present an analytical study of RCF's based on the wave function in the one-magnon approximation. This wave function is sufficient for a quantitative discussion in the large-J case; yet it also predicts the large distance behavior for smaller J values.

The main $\mathbf{k}$ dependence in the wave function stems from the hole-magnon coupling matrix element $M_{\mathbf{kq}}$. In the $q \rightarrow 0$
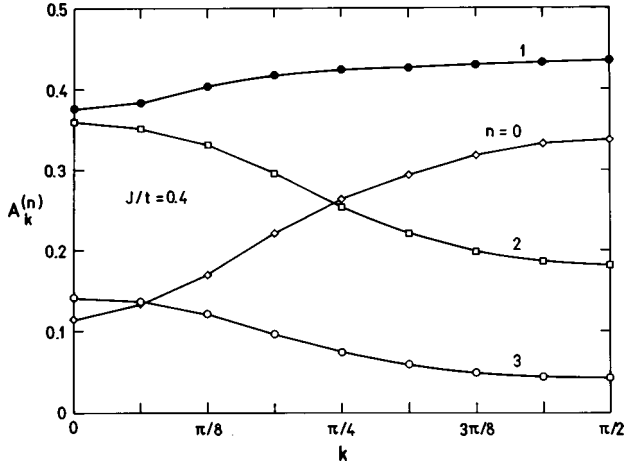
FIG. 12. Magnon distribution function $A_{\mathbf{k}}^{(n)}$ for the t-J model ($J/t=0.4$) as a function of $\mathbf{k}=(k,k)$ for various magnon numbers n: $n=0$ (diamonds) $n=1$, (full circles), $n=2$ (open squares), and $n=3$ (open circles). The numerical calculation of all matrix elements was performed on a grid corresponding to a 16×16 system. Lines connecting the symbols are guides to the eye only.

FIG. 13. The average number of magnons $\langle n \rangle$ involved in the spin-polaron formation in the t-J model as a function of J/t. The polaron momentum is $\mathbf{k}=(3\pi/8,3\pi/8)$.

limit the $\mathbf{k}$ and $\mathbf{q}$ dependences of $g_{\mathbf{k},\mathbf{q}}\propto q^{-1/2}(\gamma_{\mathbf{k}}-2^{1/2}\mathbf{v}_{\mathbf{k}}\cdot\mathbf{q}/q)$ determines the asymptotic symmetry of the correlation functions. From this structure of $g_{\mathbf{k},\mathbf{q}}$ it is clear that at $k=0$ the spatial symmetry is s wave, whereas at the minimum of the QP band at $\mathbf{k}=(\pi/2,\pi/2)$ the symmetry is determined by the dipolar term, where $\mathbf{v}_{\mathbf{k}}=\nabla_{\mathbf{k}}\gamma_{\mathbf{k}}$.[20,32]

If one is only concerned about the behavior of the wave function at large distance $\mathbf{R}$ from the position of the hole $\mathbf{R}_i$ the one-magnon contribution simplifies and one can perform the corresponding Fourier transform of $g_{\mathbf{k},\mathbf{q}}$. The Bloch representation of the wave function in the limits $t/J\rightarrow0$ and $R\rightarrow\infty$ is then approximated in leading order,

$$|\Psi_{\mathbf{k}\uparrow}^{(1)}\rangle\simeq Z_{\mathbf{k}}^{1/2}\sqrt{\frac{2}{N}}\Bigg[\sum_{\mathbf{R}_i\in\uparrow}e^{-i\mathbf{k}\cdot\mathbf{R}_i}h_{\mathbf{R}_i}^{\dagger}$$
$$+\sum_{\mathbf{R}_i\in\downarrow}e^{-i\mathbf{k}\cdot\mathbf{R}_i}h_{\mathbf{R}_i}^{\dagger}\sum_{\mathbf{R}}(\phi_0+i\phi_1)S_{\mathbf{R}_i+\mathbf{R}}^{+}\Bigg]|0\rangle.$$

(37)

Here the Fourier transforms $\phi_0=-2\sqrt{2}\gamma_{\mathbf{k}}t/(JR)$ and $\phi_1=-2(\mathbf{v}_{\mathbf{k}}\cdot\mathbf{R})t/(JR^2)$ have different spatial symmetries. The ϕ_1 term is dipolar and vanishes at $\mathbf{k}=(0,0)$ and (π,π). At $(\pi/2,\pi/2)$ ϕ_1 has its maximum, while the monopole contribution ϕ_0 vanishes instead. We note that $|\Psi_{\mathbf{k}\uparrow}^{(1)}\rangle$ has similarity to the wave function describing the motion of a ^{3}He atom in superfluid ^{4}He.[43,44] In the following this wave function will serve us as a starting point for the derivation of the asymptotic properties of various correlation functions.

The wave function [Eq. (23)] is also properly normalized for the Heisenberg limit, and the norm is given by Eqs. (24) and (25). The evaluation of $A_{\mathbf{k}}^{(n)}$ can be done numerically. In Fig. 12 $A_{\mathbf{k}}^{(n)}$ is plotted for $\mathbf{k}=(k,k)$ and $n=0$, 1, 2, and 3 at $J/t=0.4$. For $n=0$, $A_{\mathbf{k}}^{(0)}=Z_{\mathbf{k}}$, and the momentum dependence is well known.[10] The next term, $n=1$, corresponds to the emission of one magnon. The momentum dependence is
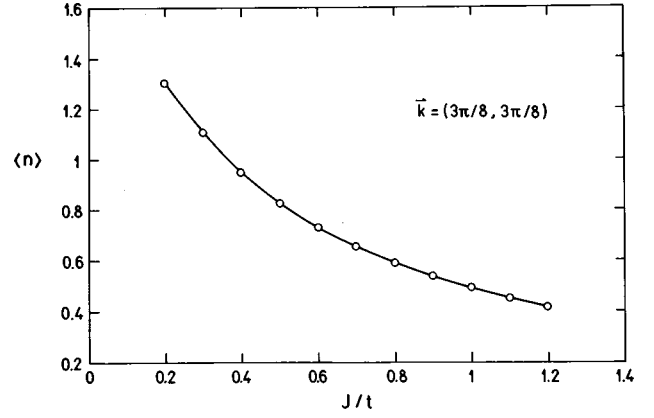
very weak, which can be qualitatively understood from the $t/J\rightarrow0$ limit. For $q<q_c\ll1$ the one-magnon contribution $A_{\mathbf{k}}^{(1)}$ follows as

$$A_{\mathbf{k}}^{(1)}|_{q_c}\simeq\frac{Z_{\mathbf{k}}}{2\pi^2}\int_0^{2\pi}d\varphi\int_0^{q_c}g_{\mathbf{k},\mathbf{q}}^2qdq\propto(\gamma_{\mathbf{k}}^2+|\mathbf{v}_{\mathbf{k}}|^2)q_c.$$

(38)

Here we have set $Z_{\mathbf{k}}\sim1$ for the weak-coupling limit. The obtained result is *constant* for $\mathbf{k}$ along the (1,1) line. This behavior is found in the full numerical calculations even in the strong-coupling regime $J/t=0.4$ in Fig. 12. Other distribution functions $A_{\mathbf{k}}^{(n)}$ in Fig. 12 have a more subtle momentum dependence which cannot be reproduced with this simple asymptotic expansion. The sum $\Sigma_{n=0}^{n=3}A_{\mathbf{k}}^{(n)}$ is close to 1, as it is clear also from Figs. 6(a) and 6(b). The results in Fig. 12 show that the higher-order magnon terms are less important for quasiparticle momenta close to the band minimum at $\mathbf{k}=(\pi/2,\pi/2)$. For the full J/t dependence of the norm at $\mathbf{k}=(\pi/2,\pi/2)$, see Ref. 20. In order to obtain converged results in the Heisenberg limit, we performed numerical calculations using unit cells with $N=16\times16$ up to $N=32\times32$. In summations over the Brillouin zone the points $q=0$ and $\mathbf{q}=\mathbf{Q}$ were excluded. The numerical method of solving the SCBA equations for $G_{\mathbf{k}}(\omega)$ was identical to Ref. 36.

The average number of magnons $\langle n \rangle$ in Fig. 13 is presented for $J/t=0.4$ and momentum $\mathbf{k}=(3\pi/8,3\pi/8)$, i.e., close to the QP band minimum. It is interesting that $\langle n \rangle$ calculated for the t-J model almost coincides with the result obtained for the Ising case (Fig. 5).

The additional spin deviations created by the hole motion are given by the expression $N_{\mathbf{R}}=\langle n_0(a_{\mathbf{R}}^{\dagger}a_{\mathbf{R}})\rangle-N_{\text{AFM}}$. Here we subtracted the large contribution $N_{\text{AFM}}=0.197$ due to the quantum fluctuations in the ground state of the 2D Heisenberg antiferromagnet in the absence of the hole. The shape of the polaron is elongated in the direction of the QP momentum which reflects a quasi-one-dimensional motion of the polaron, as was pointed out in Ref. 20. This is consistent with the asymmetry of the QP energy band in the ``hole pocket'' region centered around $\mathbf{k}=(\pi/2,\pi2)$, where the effective next-nearest-neighbor hopping for the (1,1) direction
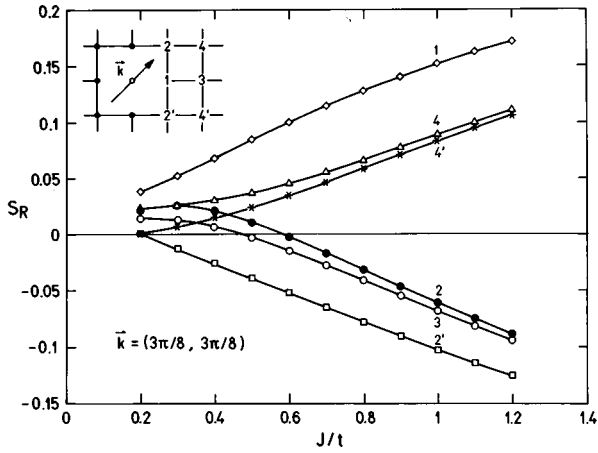
FIG. 14. The z component of the spin-correlation function $S_\mathbf{R}$ vs J/t for $\mathbf{k}=(3\pi/8, 3\pi/8)$. Note the asymmetry between the directions $\mathbf{R}\|(1,1)$ and $\mathbf{R}\|(1,-1)$ in the t-J model. The numerical calculation was performed on a grid corresponding to a 16×16 system.

is $\sim5\times$ that in the $(1,-1)$ direction. This asymmetry is most pronounced at the bottom of the QP band, and gradually vanishes away from the QP energy minimum and disappears at $k=0$ and $\mathbf{k}=(\pi,0)$. In the limit $R\rightarrow\infty$ the perturbative result is to lowest order in t/J given by

$$N_\mathbf{R}=\frac{8t^2}{J^2R^2}\left[\gamma_\mathbf{k}^2+\left(\frac{\mathbf{v}_\mathbf{k}\cdot\mathbf{R}}{R}\right)^2\right]. \qquad (39)$$

This result strictly holds only asymptotically, but nevertheless it reflects all symmetries found at short distances in the numerical treatment. The momentum dependence is qualitatively correct as well, while the J/t dependence is correct only in the range of validity of perturbation, $t/J\rightarrow0$. The correlation function $N_\mathbf{R}$ decays as a power law, $N_\mathbf{R}\propto R^{-2}$. Although the number of excited magnons $\langle n\rangle$ is small, it turns out that the change in the total number of spin deviations $\Sigma_\mathbf{R}N_\mathbf{R}$ diverges logarithmically. The definition of the polaron size used for the Ising limit of the model thus cannot be used here. Since the magnetic excitations $\omega_\mathbf{q}$ vanish linearly with q, also other correlation functions show power-law decay, yet with different exponents.[20]

In Fig. 14 we display the distribution of z component of spin $S_\mathbf{R}$ as a function of J/t and for $\mathbf{k}=(3\pi/8,3\pi/8)$. This correlation function depends strongly on the direction and size of the momentum of the quasiparticle (see Ref. 20). The asymmetry of the polaron is reflected in different values for $S_\mathbf{R}$ at positions $\mathbf{R}$ labeled with 2 and 2′ or 4 and 4′, respectively. This result is quite different from the isotropic perturbation in the Ising limit (e.g., Fig. 9). We stress that the same asymmetry was found in numerical studies of an 18-site t-J cluster with one hole.[18] The ground state is at $\mathbf{k}=(\frac{2}{3}\pi,\frac{2}{3}\pi)$ for $J/t=0.4$ [The point $\mathbf{k}=(\pi/2,\pi/2)$ is absent in that system.] Due to the high symmetry of the 4×4 cluster, such subtle asymmetries of the polaron cannot be studied there. The J/t dependence of $S_\mathbf{R}$ is in excellent agreement with the results of Refs. 3 and 4. As finite-size effects in such small clusters are expected to be quite large, the good agreement of $S_\mathbf{R}$ with the exact results is surprising. The reason for the disappearance of the AFM structure in this correlation func-

tion for small J/t is as in the Ising limit a consequence of fast hole motion which leads to an average over the two sublattices. It does not imply that the antiferromagnetic order of the spin background is destroyed. The correlation function is small in this limit because the polaron is large and many sites contribute to the sum rule $S_{tot}^z=\frac{1}{2}$.

To test our analytical and numerical procedure, we calculated $S_\mathbf{R}$ for different numbers of magnons terms n (Fig. 10). The convergence rate is similar as in the case of Ising limit, i.e., three magnon terms give a sufficient accuracy. To display the anisotropy $S_\mathbf{R}$ is shown in Fig. 10 for $\mathbf{R}=(1,\pm1)$ and $\mathbf{k}=(\pi/2,\pi/2)$ with $J/t=0.4$ as a function of number of magnon lines in the wave function, $n=1$, 2, and 3. The corresponding contributions (diagrams) are labeled with symbols (B_n) and (C_{nm}) as defined in Fig. 7. The asymmetry of the polaron, which is fully consistent with the numerical results of Ref. 18, can be attributed to the diagram C_{02}, corresponding to a two magnon process.

The effect of the hole on the AFM correlations and the energy of the spin system is measured by the nearest-neighbor spin-correlation function $C_\mathbf{R}=\langle n_0(\mathbf{S}_{\mathbf{R}_1}\cdot\mathbf{S}_{\mathbf{R}_2})\rangle$ defined on bonds between two neighboring sites $(1-2)$, $\mathbf{R}=(\mathbf{R}_1+\mathbf{R}_2)/2$.[3] In Fig. 15(a), $C_\mathbf{R}$ is shown as a function of J/t and for $\mathbf{k}=(3\pi/8,3\pi/8)$. The correlation function remains negative and in agreement with the numerical result obtained on a 16-site cluster.[3] Hence AFM correlations persist in the vicinity of the hole contrary to what one would expect from the ferromagnetic polaron picture. $C_\mathbf{R}$ is asymmetric as can be seen, e.g., from the bonds $\mathbf{R}=(1,\pm\frac{1}{2})$, labeled with 1 and 1′. The momentum dependence of $C_\mathbf{R}$ can be explained with the perturbative result which follows from asymptotic wave function Eq. (37),[20]

$$C_\mathbf{R}=-0.329+\frac{4t^2}{J^2R^4}(\gamma_\mathbf{k}^2+2|\mathbf{v}_\mathbf{k}|^2). \qquad (40)$$

This correlation function decays as R^{-4} at large distances, and could be used as a definition of the size of the polaron. Our results suggest that the size of the polaron measured with this correlation function is, at moderate $J/t=0.4$, of the order of a few lattice sites.

Another interesting aspect of the deformation of the spin background is contained in the bond-spin currents $\mathbf{j}_\mathbf{R}=\langle n_0(\mathbf{S}_{\mathbf{R}_1}\times\mathbf{S}_{\mathbf{R}_2})^z\mathbf{u}\rangle$, where $\mathbf{u}$ is a unit vector $\mathbf{u}=\mathbf{R}_2-\mathbf{R}_1$.[18,45] This quantity follows from the equation of motion for the spin density

$$\dot{\mathbf{S}}_\mathbf{R}=it\sum_{\mathbf{u},ss'}(\hat{\sigma}_{ss'}c_{\mathbf{R},s}^\dagger c_{\mathbf{R}+\mathbf{u},s'}-\text{H.c.})-2iJ\sum_\mathbf{u}\mathbf{S}_\mathbf{R}\times\mathbf{S}_{\mathbf{R}+\mathbf{u}},$$

where $\hat{\sigma}$ are Pauli spin matrices. Here the first term is the spin current induced by the hopping of the hole and the second term ($\sim\mathbf{j}_R$) describes the backflow in the spin system. Due to the broken symmetry, the total spin is not a good quantum number; therefore we consider only the z component of the current. In Fig. 15(b), $\mathbf{j}_\mathbf{R}$ is presented as a function of J/t and for $\mathbf{k}=(3\pi/8,3\pi/8)$. $\mathbf{j}_\mathbf{R}$ is an odd function with respect to the wave vector (at $k=0$). Because of symmetry it also vanishes at $\mathbf{k}=(\pi,0)$. Since the ground state has AFM long-range order, the points $\mathbf{k}$ and $\mathbf{k}+(\pi,\pi)$ are equivalent, and therefore, $\mathbf{j}_\mathbf{R}$ vanishes also at $\mathbf{k}=(\pi/2,\pi/2)$.
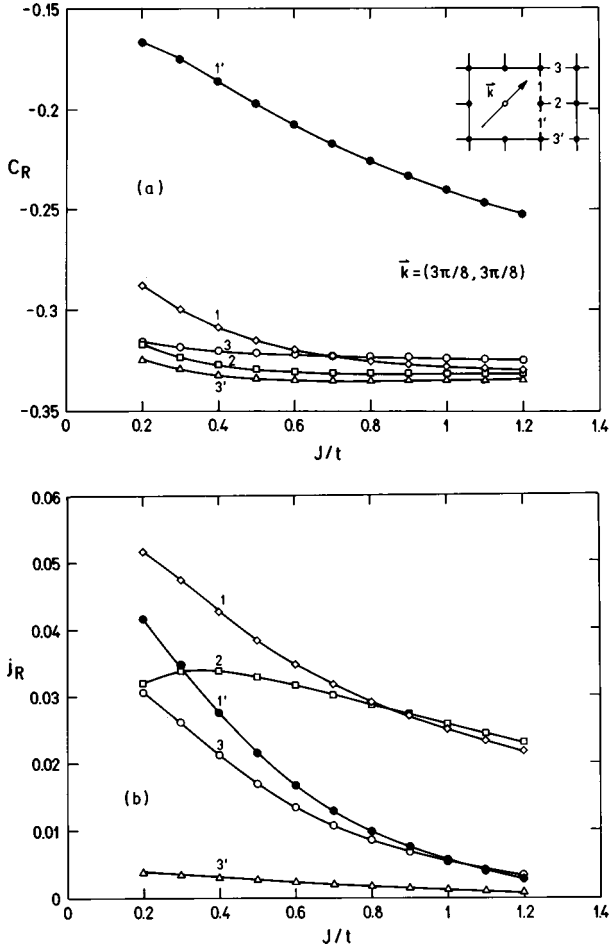
FIG. 15. (a) Nearest-neighbor spin-correlation function $C_\mathbf{R}$ and (b) the z component of the bond spin currents $\mathbf{j_R}$ as function of J/t for the quasiparticle momentum $\mathbf{k}=(3\pi/8, 3\pi/8)$. The inset in (a) provides a definition of the n.n. correlations considered. In both (a) and (b) note the asymmetry between the directions $\mathbf{R}\|(1,1)$ and $\mathbf{R}\|(1,-1)$. The asymptotic behavior is given by Eqs. (40) and (41), respectively.

Comparison of $\mathbf{j_R}$ with exact diagonalization results is delicate. As reported in Ref. 20, we find good agreement with results from Ref. 18. For the complete momentum dependence of $\mathbf{j_R}$ in comparison with exact diagonalization, see Ref. 46. Agreement is excellent in the anisotropic limit $\alpha < 1$. In the Heisenberg limit a reliable comparison is very difficult because of the strong $\mathbf{k}$ dependence of $\mathbf{j_R}$, which makes it very sensitive to the boundary conditions of small clusters. In Fig. 15(b) we present $j_\mathbf{R}$ for various bonds $\mathbf{R}$ defined in Fig. 15(a). The asymptotic pattern of bond-spin currents is dipolar,[20]

$$ j_\mathbf{R} = \frac{4\sqrt{2}t^2}{J^2 R^3}\, \gamma_\mathbf{k}\left[\mathbf{v_k} - \frac{(\mathbf{v_k}\cdot\mathbf{R})\mathbf{R}}{R^2}\right]\cdot\mathbf{u}. \qquad (41) $$

The spin backflow current $\mathbf{j_R}$ decays as R^{-3}, and vanishes in the ground state for $\mathbf{k}=(\pi/2,\pi/2)$. Again, the general momentum dependence is correct as in the case of the other correlation functions considered.

VI. CONCLUSIONS

We have outlined a method that allows one to calculate the real-space structure of a spin polaron in a quantum antiferromagnet. The approach is based on the spin-polaron formulation for the t-J model, where holes are described as spinless fermions, while the spin excitations are treated within linear spin-wave theory. The single-particle Green's function in the (self-consistent) Born approximation, which was shown earlier to provide an excellent description of the numerical data for the t-J model, is sufficient to calculate the many-body wave function describing the polaron (Reiter's wave function). We have shown here how this wave function can be used to calculate quite complex correlation functions in the framework of the self-consistent Born approximation.

Our calculation of a number of correlation functions, which measure the deformation of the spin system due to a moving hole (spin polaron), provides a very detailed check of this approach against exact diagonalization. In particular, we have shown that the spectral weight of the spin-polaron quasiparticle calculated from the wave function is consistent with the result derived from the Green's function. It is demonstrated how the number of spin excitations involved in the polaron formation increases with decreasing spin stiffness when $J\to 0$. We have determined the probability distribution of the number of magnons excited in the ground state and found that for $J/t = 0.4$ (a typical value for copper-oxide superconductors) the average number of magnons is about one. In the Ising limit the average number of magnons scales as $\langle n\rangle \propto (t/J^z)^{1/3}$ as $J^z/t\to 0$, in agreement with the string picture for the moving hole and with Ref. 41.

We have put particular emphasis on the asymptotic decay of the perturbations introduced by spin-polaron formation. Since the spin-wave energies $\omega_\mathbf{q}$ in a quantum antiferromagnet vanish linearly with q, perturbations in the spin system decay with a power law, for example, the change of the local spin deviations $N_\mathbf{R}\propto R^{-2}$, while the perturbation of the nearest-neighbor spin correlations decays as R^{-4} with the distance from the hole. In the t-J model all correlation functions have a quite complex structure in real space which depends on the momentum of the polaron, whereas in the t-J^z model all perturbations are isotropic.

We note that despite the power-law decay of the polaron correlation functions in the t-J model, the quasiparticle spectral weight does not vanish. Whether this is correct or an artifact of the self-consistent Born approximation remains to be shown by a more rigorous treatment. Finally we want to stress that the approach discussed here may also be applied to other interesting problems such as strongly correlated electrons coupled to Holstein or other phonons.

[1] For recent reviews, see E. Dagotto, Rev. Mod. Phys. **66**, 763 (1994); Yu. A. Izyumov, Usp. Fiz. Nauk **167**, 465 (1997) [Phys. Usp. **40**, 445 (1997)].

[2] K. J. von Szczepanski, P. Horsch, W. Stephan, and M. Ziegler, Phys. Rev. B **41**, 2017 (1990); P. Horsch *et al.*, Physica C **162-164**, 783 (1989).

[3] J. Bonča, P. Prelovšek, and I. Sega, Phys. Rev. B **39**, 7074 (1989).

[4] Y. Hasegawa and D. Poilblanc, Phys. Rev. B **40**, 9035 (1989).

[5] E. Dagotto, R. Joint, A. Moreo, S. Bacci, and E. Gagliano, Phys. Rev. B **41**, 9049 (1990).

[6] D. Poilblanc, T. Ziman, H. J. Schulz, and E. Dagotto, Phys. Rev. B **47**, 14 267 (1993).

[7] P. W. Leung and R. J. Gooding, Phys. Rev. B **52**, R15 711 (1995).

[8] S. Schmitt-Rink, C. M. Varma, and A. E. Ruckenstein, Phys. Rev. Lett. **60**, 2793 (1988).

[9] C. L. Kane, P. A. Lee, and N. Read, Phys. Rev. B **39**, 6880 (1989).

[10] G. Martínez and P. Horsch, Phys. Rev. B **44**, 317 (1991).

[11] J. Igarashi and P. Fulde, Phys. Rev. B **45**, 10 419 (1992).

[12] S. A. Trugman, Phys. Rev. B **37**, 1597 (1988).

[13] R. Eder and K. W. Becker, Z. Phys. B **78**, 219 (1990).

[14] P. Prelovšek, I. Sega, and J. Bonča, Phys. Rev. B **44**, 317 (1990).

[15] Z. B. Su, Y. M. Li, W. Y. Lai, and L. Yu, Phys. Rev. Lett. **63**, 1318 (1989).

[16] J. A. Riera and E. Dagotto, Phys. Rev. B **55**, 14 543 (1997).

[17] H. Barentzen, Phys. Rev. B **53**, 5598 (1996).

[18] V. Elser, D. A. Huse, B. I. Shraiman, and E. D. Siggia, Phys. Rev. B **41**, 6715 (1990).

[19] B. I. Shraiman and E. D. Siggia, Phys. Rev. Lett. **60**, 740 (1988); **61**, 467 (1988).

[20] A. Ramšak and P. Horsch, Phys. Rev. B **48**, 10 559 (1993).

[21] B. O. Wells *et al.*, Phys. Rev. Lett. **74**, 964 (1995).

[22] T. Tohyama and S. Maekawa, Phys. Rev. B **49**, 3596 (1994); J. Bała, and A. M. Oleś, *ibid.* **52**, 4597 (1995); A. Nazarenko *et al.*, *ibid.* **51**, 8676 (1995); B. Normand and P. A. Lee, *ibid.*, **51**, 15 519 (1995); V. I. Belinicher *et al.*, *ibid.* **54**, 14 914 (1996); N. M. Plakida *et al.*, *ibid.* **55**, R11 997 (1997).

[23] O. A. Starykh *et al.*, Phys. Rev. B **52**, 12 534 (1995); J. Bała, A. M. Oleś, and J. Zaanen, *ibid.* **54**, 10 161 (1996); F. Lema and A. A. Aligia, *ibid.* **55**, 14 092 (1997).

[24] L. N. Bulaevski, E. L. Nagaev, and D. I. Khomskii, Zh. Éksp. Teor. Fiz. **54**, 1562 (1968) [Sov. Phys. JETP **27**, 836 (1968)].

[25] F. Brinkman and T. M. Rice, Phys. Rev. B **2**, 1324 (1970).

[26] P. W. Anderson, Science **235**, 1196 (1987).

[27] P. W. Anderson, Phys. Rev. Lett. **64**, 1839 (1990).

[28] Z. Y. Weng, D. N. Sheng, Y. C. Chen, and C. S. Ting, Phys. Rev. B **55**, 3894 (1997).

[29] N. M. Plakida, V. S. Oudovenko, and V. Yu. Yushankhai, Phys. Rev. B **50**, 6431 (1994).

[30] A. Sherman and M. Schreiber, Phys. Rev. B **50**, 12 887 (1994).

[31] N. M. Plakida, V. S. Oudovenko, P. Horsch, and A. I. Liechtenstein, Phys. Rev. B **55**, R11 997 (1997).

[32] G. F. Reiter, Phys. Rev. B **49**, 1536 (1994).

[33] A. Ramšak, P. Horsch, and P. Fulde, Phys. Rev. B **46**, 14 305 (1992).

[34] B. Kyung, S. I. Mukhin, V. N. Kostur, and R. A. Ferrell, Phys. Rev. B **54**, 13 167 (1996).

[35] P. Horsch and A. Ramšak, J. Low Temp. Phys. **95**, 343 (1994).

[36] A. Ramšak and P. Prelovšek, Phys. Rev. B **42**, 10 415 (1990).

[37] N. Bulut, D. Hone, D. J. Scalapino, and E. Y. Loh, Phys. Rev. Lett. **62**, 2192 (1989).

[38] A. G. Mal'shukov and G. D. Mahan, Phys. Rev. Lett, **68**, 2200 (1992).

[39] Z. Liu and E. Manousakis, Phys. Rev. Lett. **45**, 2425 (1992).

[40] E. Dagotto and J. R. Schrieffer, Phys. Rev. B **43**, 8705 (1991).

[41] D. C. Mattis and H. Chen, Int. J. Mod. Phys. B **5**, 1401 (1991).

[42] Y. Nagaoka, Phys. Rev. **147**, 392 (1966).

[43] R. P. Feynman and M. Cohen, Phys. Rev. **102**, 1189 (1956); W. L. McMillan, *ibid.* **175**, 266 (1968).

[44] F. Marsiglio, A. E. Ruckenstein, S. Schmitt-Rink, and C. M. Varma, Phys. Rev. B **43**, 10 882 (1991).

[45] J. Inoue and S. Maekawa, J. Phys. Soc. Jpn. **59**, 2119 (1990); **59**, 3467 (1990).

[46] A. Ramšak, P. Horsch, and J. Jaklič, Physica C **235-240**, 2247 (1994).